The impact of a land-sea contrast on convective aggregation in radiative-convective equilibrium

Beth Dingley[1], Guy Dagan[2], Philip Stier[1], Ross Herbert[1]

[1]Atmospheric, Oceanic and Planetary Physics, Department of Physics, University of Oxford
[2]The Hebrew University of Jerusalem, Israel

Key Points:

- Convection preferentially aggregates over land in a global radiative-convective equilibrium simulation
- A global land-centered circulation drives the aggregation and is triggered through surface fluxes, but maintained through longwave fluxes
- The land-based convective cluster appears to have a maximum spatial scale of 10,000 km

Corresponding author: Beth Dingley, elisabeth.dingley@physics.ox.ac.uk

Abstract

Convective aggregation is an important atmospheric phenomenon which frequently occurs in idealised models in radiative-convective equilibrium (RCE), where the effects of land, rotation, sea surface temperature gradients, and the diurnal cycle are often removed. This aggregation is triggered and maintained by self-generated radiatively driven circulations, for which longwave feedbacks are essential. Many questions remain over how important the driving processes of aggregation in idealized models are in the real atmosphere. We approach this question by adding a continentally-sized, idealized tropical rainforest island into an RCE model to investigate how land-sea contrasts impact convective aggregation and its mechanisms. We show that convection preferentially forms over the island persistently in our simulation. This is forced by a large-scale thermally driven circulation. First, a sea-breeze circulation is triggered by the land-sea thermal contrast, driven by surface sensible heating. This sea-breeze circulation triggers convection which then generates longwave heating anomalies. We find that these longwave heating anomalies are essential for maintaining the aggregation of convection over the island through mechanism denial tests. We also show, by varying the island size, that the aggregated convective cluster appears to have a maximum spatial extent of 10,000 km. These results highlight that the mechanisms of idealized aggregation remain relevant when land is included in the model, and therefore these mechanisms could help us understand convective organization in the real-world.

Plain Language Summary

Large storm clouds that often form in the tropical atmosphere can cluster together to form cloud systems, which are associated with large amounts of precipitation within the cloudy region, and very dry conditions away from the cloudy region. These cloud systems - known as organized deep convection - are often studied in simplified models of the atmosphere where the land, Earth's rotation, variations in sea-surface temperature, and the diurnal cycle are removed. The simplified models allow scientists to understand the processes

driving deep convection and why it organizes into these large systems. Using these models in previous studies has helped us understand that interactions between the atmosphere, the clouds and longwave radiation have an important role in organizing convection.

In this paper we take a step towards reality and look at how including a large, idealized island in one of these simplified models affects how convection organizes together. We show that convective clouds will group together over the land throughout our model simulations, and that the processes driving this are similar to those organizing convection in previous papers. The results shown in the paper highlight that results from idealized modelling studies could help us understand how convection organizes in the real-world.

1 Introduction

In the tropics, deep convection transports large amounts of water vapour and energy vertically, as well as playing an important role in setting the Earth's radiative budget and large-scale circulations. This deep convection can be organized on a range of scales, from mesoscale convective systems, up to planetary envelopes of convection like the Madden-Julian Oscillation (MJO) (Madden & Julian, 1994; Tobin et al., 2012). Organized systems like these provide a significant contribution to tropical precipitation and cloudiness, with a large fraction of precipitation extremes occurring during convective organization (Roca & Fiolleau, 2020). Increased convective clustering has also been shown to affect large-scale circulations, including the structure and extent of the intertropical convergence zone (Popp & Bony, 2019).

Idealized climate models are a useful tool for studying moist convection in the tropical climate. In these models rotation, land, the diurnal cycle, and sea surface temperature (SST) gradients are often removed. This simplified configuration is known as radiative-convective equilibrium (RCE), where any imbalances in radiative cooling are balanced by convective heating (Manabe & Wetherald, 1967). Removing these complexities associated

with heterogeneities in the boundary conditions allows for studies to analyse the processes of importance to moist convection, such as its interactions with radiation and circulations (Wing et al., 2020). Due to the negligible Coriolis force in the tropics, previous studies have found that RCE is a reasonable representation of the tropical climate (Jakob et al., 2019), and therefore it has been extensively used in studies on the tropical atmosphere (e.g Manabe & Wetherald, 1967; Held et al., 1993; Tompkins & Craig, 1998; Robe & Emanuel, 2001; Stephens et al., 2008; Khairoutdinov & Emanuel, 2013; Wing et al., 2020).

In many models using an RCE configuration, deep convection has been found to spontaneously cluster together through radiatively-driven circulations, despite homogeneous boundary conditions; a phenomenon called convective self-aggregation (Held et al., 1993; Tompkins & Craig, 1998; Bretherton et al., 2005; Muller & Held, 2012; Wing & Emanuel, 2014; Coppin & Bony, 2015; Wing et al., 2020). The self-aggregation of convection has been found to require longwave radiative feedbacks for its initiation and maintenance, with shortwave and surface enthalpy feedbacks being shown to contribute to the aggregation's initiation, but ultimately have been found to not be essential for aggregation to form (Wing & Emanuel, 2014; Coppin & Bony, 2015; D. Yang, 2018a; Muller & Held, 2012).

Despite RCE being regarded as a reasonable simplification of the tropical climate, the real-world relevance of the behaviour of deep convection in these models is debated. In particular, many of the processes which are removed in an RCE model have been shown to influence the organization of convection, such as SST gradients (Tompkins & Semie, 2017; Shamekh et al., 2020a; Müller & Hohenegger, 2020) and land-sea contrasts (Sato et al., 2009; Leutwyler & Hohenegger, 2021; Cronin et al., 2015). There are an increasing number of studies which highlight the possible role of the feedbacks essential to aggregation in real-world convective processes. For example, both the MJO and tropical cyclones have been simulated in RCE models with rotation (Arnold & Randall, 2015; Khairoutdinov & Emanuel, 2018; Davis, 2015; Wing et al., 2016; Muller & Romps, 2018), and the diabatic

heating from absorbing aerosol plumes has been shown to force convection to aggregate (Dingley et al., 2021). Inhomogeneous surfaces have also been shown to strongly affect convective aggregation. Studies have shown that SST gradients force convection to cluster over warmer SSTs (Tompkins, 2001; Shamekh et al., 2020a; Müller & Hohenegger, 2020), whilst interactive SSTs have been shown to prevent or delay the aggregation of convection (Hohenegger & Stevens, 2016; Shamekh et al., 2020b). This is because the SST under a convective cluster will cool due to cloud shielding, whilst SSTs away from the convection will warm, which will then drive a circulation towards the dry region, disaggregating the convection. The organization of convection has also been studied on a land-like planet in RCE, with no ocean. Here Hohenegger & Stevens (2018) found that, as with interactive SSTs, the ability of land to change temperature causes a homogenization of the precipitation field on long time scales. They found that when an area of the domain is not covered by a convective cluster, the drying which occurs acts to induce a low-level circulation which changes the low-level flow direction towards this dry region, instead of towards the convective cluster. This aggregates convection in this originally drier region, until a new dry area forms and induces this circulation reversal again. Therefore, these soil moisture-atmosphere interactions can act to prevent the long-term aggregation of convection.

Aggregation that occurs with inhomogenous boundary conditions (such as SST gradients, land, or aerosol plumes) is no longer referred to as 'self-aggregation', due to the external processes which now are responsible for forcing the clustering. In these forced aggregation cases, it has has been shown that convection can sometimes aggregate in the absence of the usually essential longwave radiative feedbacks (Shamekh et al., 2020a; Dingley et al., 2021), generally due to a temperature gradient being maintained via an external diabatic process, such as a hot-spot in the SST (Shamekh et al., 2020a), or the radiative perturbation from an aerosol plume (Dingley et al., 2021). These inhomogeneities can then drive a thermally-driven circulation and aggregate the convection.

Thus far, less attention has been given to the impact of land-sea contrasts on aggregation. Differences in the behaviour of land and ocean could have large impacts on aggregation, such as the differences in the heat capacities of land and ocean (causing the land-ocean thermal contrast), moisture availability (land has the ability to dry out, whereas the ocean acts as an infinite water source), orography and the surface roughness length. Each of these factors can greatly affect the surface fluxes, which have previously been shown to impact the formation of aggregation (Bretherton et al., 2005; Coppin & Bony, 2015; D. Yang, 2018a), and so including land in RCE simulations could impact whether aggregation can form, and its lifetime, whilst also taking a large step towards a more realistic modelling paradigm.

Previous investigations of islands in an RCE model have shown that convection and precipitation tend to favor land (Cronin et al., 2015; Leutwyler & Hohenegger, 2021; Coppin & Bellon, 2019; Wang & Sobel, 2017). Land has also been found to have an impact on the domain-mean tropospheric temperature in an RCE simulation. Cronin et al. (2015) found that the presence of an island increased the tropospheric temperature comparatively to an all-ocean simulation, and this warming increased monotonically with island size. They postulate that this is due to the clouds forming at the warmest and moistest areas (which are over the island), pushing deep convection towards a moister adiabat. Contrastingly, Leutwyler & Hohenegger (2021) found that the presence of islands has a tendency to cool the troposphere, with larger islands having a larger cooling effect. They hypothesise that the reason their result contradicts that of Cronin et al. (2015) is due to a difference in modelling design: Cronin et al. (2015) model the land simply by changing the ocean's heat capacity, and so in their model there is no limit on water availability, whereas Leutwyler & Hohenegger (2021) use a land surface scheme which allows for soil drying. Therefore, in the absence of precipitation, the soil is able to dry out, limiting evaporation, and thus drying the sub-cloud layer. These contradicting results could benefit from additional exploration, which we will provide in this paper.

Previous studies of islands in an RCE simulation have focused mainly on the effect the land-sea contrast has on the diurnal cycle, precipitation and temperature profile more than the mechanisms behind any organization of convection. They have also exclusively investigated the effect in a cloud-resolving model (CRM), where island size is limited. To our knowledge, no studies thus far have investigated the effect of a larger, continentally-sized island and its impacts on aggregation. In this paper we aim to answer the following questions:

1. How does the inclusion of an idealized island in a global RCE model impact the aggregation of convection? In particular:
   - the spatial structure of aggregation,
   - the domain-mean atmospheric properties.
2. How does the inclusion of an island affect the global circulation?
3. Are the physical mechanisms responsible for aggregation similar to those seen in land-free simulations, or forced aggregation simulations?
4. How sensitive are these results to the island size?

2 Methods

2.1 Model set-up

We employ the ICOsahedral Nonhydrostatic Atmospheric GCM (ICON; Giorgetta et al. 2018; Zängl et al. 2015), version 1.8, coupled to the JSBACH4 land model (Jungclaus et al., 2022) in all simulations described in this paper. This version of the ICON GCM model uses the ECHAM6 physics packages (for a full description, see Stevens et al., 2013), including a bulk mass-flux convection scheme (Nordeng, 1994; Tiedtke, 1989) and cloud cover calculated using the relative humidity (Sundqvist et al., 1989). Other parameterisation schemes used are the Lohmann and Roeckner microphysics scheme (Lohmann & Roeckner, 1996) and the gravity wave scheme as described in Stevens et al. (2013).

The JSBACH4 land model is a dynamic global vegetation model and offers a full representation of soil-vegetation-atmosphere interactions. The surface energy budget and soil thermal layers over land are implicitly coupled to ICON through the vertical diffusion scheme. There are five soil layers which descend to 10 m depth; heat and water dynamics are defined on these soil levels.

ICON is run on a triangular grid, based on dividing a spherical icosahedron. In this paper we use the R02B04 grid, which has 20480 cells, with an average cell area of approximately 25000 km^2, and an approximate equivalent grid-spacing of 160 km. Each grid cell over land is divided into two sections: a "tiled" fraction, and the fraction of the non-ice covered grid-cell that is inhospitable to vegetation (for example, rocky terrain or sandy desert). The tiled fraction of the grid box is then further separated into different surface types to represent sub-grid scale heterogeneity: a glacier, or one of 11 plant functional types (Reick et al., 2013). In our simulations, all land grid cells are completely covered by vegetation, with no glaciers, to mimic warm tropical conditions. The vertical resolution is set by assigning 47 stretched model levels between the surface and model top at 83 km, with grid spacings ranging from 40 m between the lowest model layers, to around 1350 m at 15 km, and 5900 m near the model top. In these simulations we use a model time step of 15 minutes, with radiation calculated every 90 minutes.

2.2 Experimental set-up

ICON is used in an RCE configuration. The simulations are setup with no rotation, no diurnal cycle, no large-scale imposed winds, and a fixed SST of 305K, an SST where strong self-aggregation occurs in the ICON GCM (Dingley et al., 2021). The RCE state is initialized from homogenised boundary conditions with a solar insolation of 551.58 Wm^{-2} and a fixed zenith angle of 42.05° giving a constant total insolation of 409.6 Wm^{-2}, equivalent to the annual mean insolation in the tropics. The temperature and specific humidity profiles

are initialized from a one month, non-aggregated aquaplanet simulation: we use horizontal means of the temperature and humidity profiles at the end of this non-aggregated simulation, and add some noise in the lowest five layers (see Wing et al., 2018), then set those profiles as our initial conditions in the remaining simulations. The ocean albedo is set to 0.07. Concentrations of tracers CO2, CH4, N2O and O2 are set to be constant in space and time and the O3 profile is the same as used in Popke et al. (2013). This atmospheric configuration follows that of the RCE model intercomparison (RCEMIP) project (Wing et al., 2018). The simulations described in this paper were run for two years.

Land in our simulations is represented by a large, tropical-like, circular island, located at latitude = 0° longitude = 0° with a radius of 40° (giving the land an area of $35.7*10^6$ km^2). Surface properties have been set to average tropical rainforest-like values, with tropical broadleaf evergreen vegetation covering the island. Rainforest surface properties are taken from the JSBACH4 initialization dataset (Hagemann, 2002; Reick et al., 2021), and averaged over a box in the Amazon with latitudes ranging between -1° to -10° and longitudes ranging between -70° to -60°. Some of the key surface properties are listed in Table 1. Soil temperature is the only property not set using Amazon rainforest equivalent values. Soil temperature is initialized as equal to the SST at all model levels, following Leutwyler & Hohenegger (2021). We ran a test simulation with Amazon rainforest values for the soil temperature and found that our results were invariant to this choice. Results were also tested with island surface temperatures ranging between 300K to 310K at increments of 1K, and again were found to be invariant to our choice of initial temperature. The island has an elevation of 0 m everywhere, to remove effects on convection and its organization from topography.

Here, we describe three simulation setups which differ from the standard simulation described thus far. Firstly, the results from the land simulation we run are compared to an aggregated 'no land' RCE simulation (hereafter referred to as NoLand-Aggregated).

Parameter Name	*Value*
Soil type	Mixture of loam and clay
Leaf area index	8.928
Root depth	1.351 m
Vegetation albedo	0.122
Roughness length	1.871 m
Soil depth (to bedrock)	2.194 m
Heat capacity	$2.296{*}10^6$ $\mathrm{Jm^{-3}K^{-1}}$

Table 1: Surface properties used to initialize the JSBACH4 land model within the ICON GCM

This NoLand-Aggregated RCE simulation is run on an aquaplanet, but is otherwise identical to the land simulation described above. Comparing the results from the land and NoLand-Aggregated simulations allows us to decipher what effect the land is having on the aggregation of convection. Secondly, in order to perform mechanism denial tests, we will occasionally refer to homogenized radiation runs. In these simulations, we horizontally homogenize radiative heating rates at each model level and timestep, following Muller & Held (2012). Finally, results are also often compared to a non-aggregated simulation (hereafter referred to as NoLand-NotAggregated), in order to isolate the impacts aggregation is having on the atmosphere. This NoLand-NotAggregated simulation mirrors the NoLand-Aggregated RCE simulation, but with horizontally homogenized longwave radiative heating rates, in order to prevent the convection aggregating (e.g. Arnold & Putman, 2018; Muller & Held, 2012; Wing & Emanuel, 2014).

In order to compare the aggregated state of different simulations, we use a metric of aggregation. In this paper, our metric is the variance of column-integrated relative humidity (CRH; σ^2_{CRH}) (Wing & Cronin, 2016). Column relative humidity is defined as the density-weighted integral of tropospheric precipitable water divided by the density-weighted integral of the saturated precipitable water. This metric utilizes the signature of aggregation where moist regions moisten and dry regions get drier as convection clusters together, causing

a broadening of the moisture distribution. Please note that this metric does not have a threshold value above which convection is considered as aggregated. Instead, it is used a comparative metric which allows us to compare the relative degree of aggregation across different simulations.

3 Results

3.1 Land-centered aggregation

Convection primarily forms over the island throughout our simulations (Figure 1a, c), driving large moisture gradients, with the moistest columns of the domain consistently over the island, and the driest columns tending to be the ones furthest away from the island (Figure 1b, d). This aggregated state is visually reached approximately between 5-10 days after the simulation start, although atmospheric equilibrium and therefore equilibrium in the moisture variance is reached approximately 70 days after simulation start (Figure 2). We can also see in Figure 1c that most convection which forms over the ocean subsequently gets advected towards the island, represented as the diagonal white lines (for example starting at longitude=100° at approximately day 80) slanted towards the island. Convection which is triggered over the island itself, typically forms at the centre of the island and is advected towards the coastline of the island. Videos of the OLR and CRH over the first six months can be seen in movie S1.

Figure 2 shows a comparison of the domain-mean properties of this simulation with the NoLand-NotAggregated simulation, and the NoLand-Aggregated simulation. We can see that comparatively to the NoLand-NotAggregated simulation, there is a strong domain-mean warming, free-tropospheric drying, and a decrease in high level clouds. This is consistent with the results of many previous studies (e.g. Wing et al., 2020; Cronin & Wing, 2017). The aggregated simulation with land shows similar domain-mean effects of aggregation to the NoLand-Aggregated simulation, with Figure 2a showing the same degree of aggregation

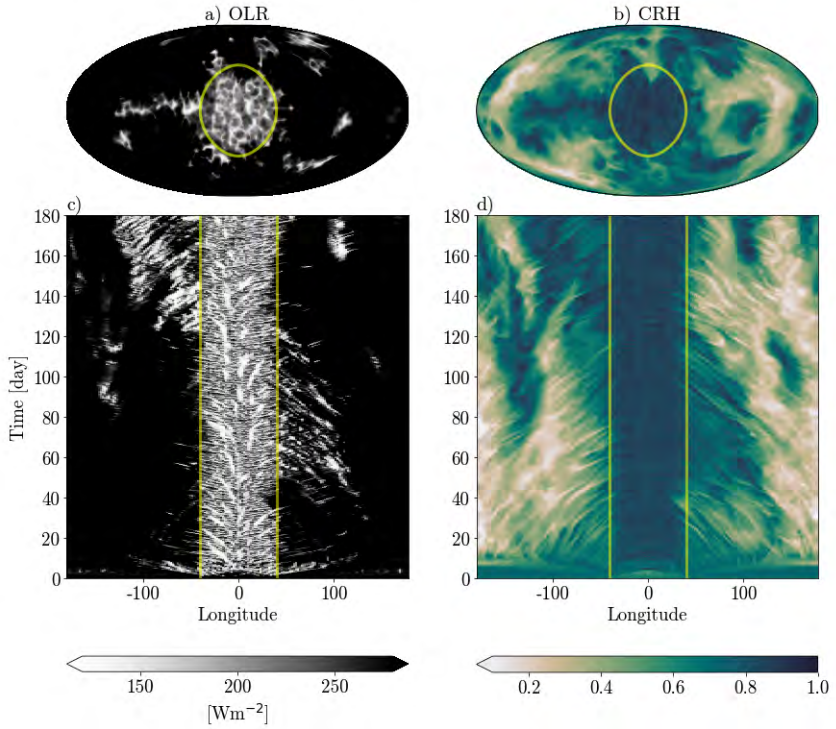

Figure 1: a), b): 4-hour mean snapshots of a) outgoing longwave radiation (OLR) and b) column relative humidity (CRH) 180 days after simulation start. c), d): Hovmöller plots of c) OLR, and d) CRH over the first 180 days of the simulation, taken as a zonal slice through latitude=0°. The yellow lines show the coasts of the island.

between these two simulations. There is also little change in the amount of free-tropospheric drying and reduction in high cloud fraction between the runs with/without land, but there is slightly less drying of the lower troposphere and an increase in tropopause height when land is present. Despite these similarities between the simulations with/without land, there is a much stronger domain-mean warming throughout the troposphere in the simulation with land. This would happen, if the convection in the simulation with land is on a warmer moist adiabat than the convection in the simulation without land. This is true in our simulations as the experiment with land has convection forming over a warmer lifting condensation level than the experiment with no land. Our result here agree with Cronin et al. (2015), but not with Leutwyler & Hohenegger (2021). We hypothesise that the difference between our study and Leutwyler & Hohenegger (2021) is that their convection doesn't always remain over the island. This allows the soil to dry out which limits evaporation and results in their sub-cloud layer being drier than over the ocean, meaning that the deep convection ends up on a colder adiabat. This difference in spatial pattern of convection is likely due to Leutwyler & Hohenegger (2021) including a diurnal cycle in their simulations. The solar diurnal cycle has been shown to strongly affect the patterns of precipitation and convection over tropical islands (e.g. Wang & Sobel, 2017; Coppin & Bellon, 2019) and tropical continental land masses (e.g. G.-Y. Yang & Slingo, 2001), and so it is likely that the inclusion of a diurnal cycle would have an impact on the consistency of convection we see over the island in our simulations.

It is clear from Figure 1 that there is a large-scale circulation being generated and maintained over the island, and that this is likely responsible for the aggregation of convection throughout our simulation. It has been shown before that the self-aggregation of convection is driven by self-generated radiative circulations. These circulations have often been shown to start as an anomalous patch of dry sky, which then grows and pushes the convection to cluster together (Muller & Held, 2012; Muller & Bony, 2015; Coppin & Bony, 2015; Holloway & Woolnough, 2016), a mechanism for which longwave radiative feedbacks

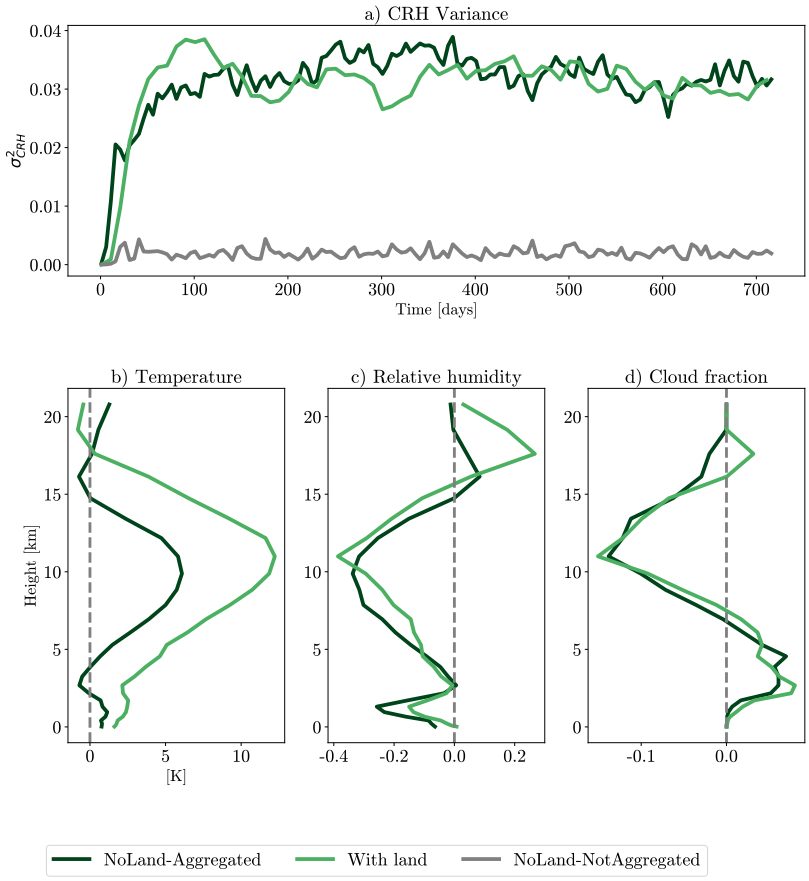

Figure 2: a) Time evolution of variance of domain-mean column relative humidity (CRH; σ^2_{CRH}). b)-d): Domain-mean vertical profiles of b) temperature, c) relative humidity, d) cloud fraction, time-averaged over days 100-720 of the simulations. In all plots dark green lines represent a self-aggregated RCE simulation with no land ('NoLand-Aggregated'), light green lines represent an aggregated RCE simulation with land, and grey lines represent a non-aggregated simulation with no land ('NoLand-NotAggregated'). For figures b)-d), the vertical profiles from the non-aggregated simulation are subtracted from the 'no land' and 'land' aggregated simulations' profiles.

are generally essential both for triggering and maintenance. We investigate here whether the convection is aggregated through the same mechanisms as self-aggregation. We will study this first by discussing the thermodynamics responsible for triggering the circulation, and then for maintaining the circulation.

Figure 3 shows some of the key physical quantities driving the circulation over the first 40 days of our simulation. Figure 3a illustrates the aforementioned circulation, and its extent. We can see that the surface winds are converging towards the island at every oceanic point, with approximate speeds of 3 ms^{-1} once aggregation has been reached (roughly 10 days after simulation start). This circulation is being triggered initially by very strong sensible heat flux anomalies at the start of the simulation, driving high near-surface temperature anomalies. These anomalies cause strongly negative boundary layer (here boundary layer is defined as the lowest 1 km) density anomalies (Figure 3b), and hence strongly positive buoyancy anomalies over the island. The land-sea thermal contrast begins to cause surface winds to converge bringing cool, dense oceanic air over the island. The circulation described here is analogous to the well documented sea-breeze circulation (Miller et al., 2003). The advected dense oceanic air elevates the warmer, more buoyant air hence triggering convection. This convection starts at the edge of the island, and as the surface circulation grows in strength, moves inwards until the whole island is covered by convecting air (Figure 3d). For a more zoomed in version of Figure 3, please see Figure S1. It is becoming increasingly clear in the field that boundary layer feedbacks are essential for triggering aggregation (e.g. Muller & Bony, 2015; Naumann et al., 2017; D. Yang, 2018b,a; Dingley et al., 2021), and our results support this hypothesis. The convection over the island triggers a gravity wave propagating at 30 ms^{-1} at 500 hPa, which acts to eliminate horizontal density gradients in the free-troposphere. This gravity wave is responsible for propagating the temperature of the warmer moist adiabat that the convection is on to the rest of the domain, consistent with the weak temperature gradient approximation (Sobel et al., 2001; Leutwyler & Hohenegger, 2021), and can be seen in Figure 3, especially in Figure 3d as a wave of subsiding air moving

outwards away from the island. The subsidence associated with this wave causes a strong drying of the columns far away from the island (Figure 1d), which completes the process of aggregation. Figures 3g and h show that in the initial two day period during which this circulation is being spun-up, the horizontal anomalies in both column longwave and shortwave radiative fluxes are minimal. Thus, it seems from Figure 3 that the circulation which aggregates the convection is triggered in this simulation with land primarily through surface fluxes, mostly the sensible heat flux, not radiative feedbacks as in previous aggregation studies. Once the convection starts to form, the longwave radiative anomalies start to grow, implying that longwave feedbacks play an important role in our circulation, but are not important for the circulation to be triggered initially. Similarly, once the dry patches away from the island form, shortwave convergence anomalies grow quite strong (Figure 3h), again implying that shortwave feedbacks play a role in amplifying the circulation.

We now turn to investigating the mechanisms responsible for maintaining this circulation. In particular, we are interested in why the convection does not disaggregate, despite the cold, dense surface air underneath the formed convective cluster. Figure 4 shows some time averaged, zonal cross-sections of various physical quantities. Figure 4a again shows the global circulation that is keeping the convection aggregated together, i.e. surface convergence towards the island center with strong upper tropospheric divergence away from the island. Figure 4b shows the vertical motions associated with convection. Inspecting the 3d temperature anomalies (Figure 4c) reveals that the near-surface negative temperature anomalies in Figure 3c are confined to less than 1 km above the surface. Above this, there is still a temperature gradient with warmer anomalies over the island than ocean, and therefore the circulation aggregating the convection is still being thermally driven. However, initially this circulation was being driven by the land-sea thermal contrast caused by the land surface heating up. This poses the question, what is now driving the thermal anomalies over the island? Figure 4d illustrates the strong gradients in longwave heating anomalies in the lower troposphere, which are positive over the island and negative away from the island.

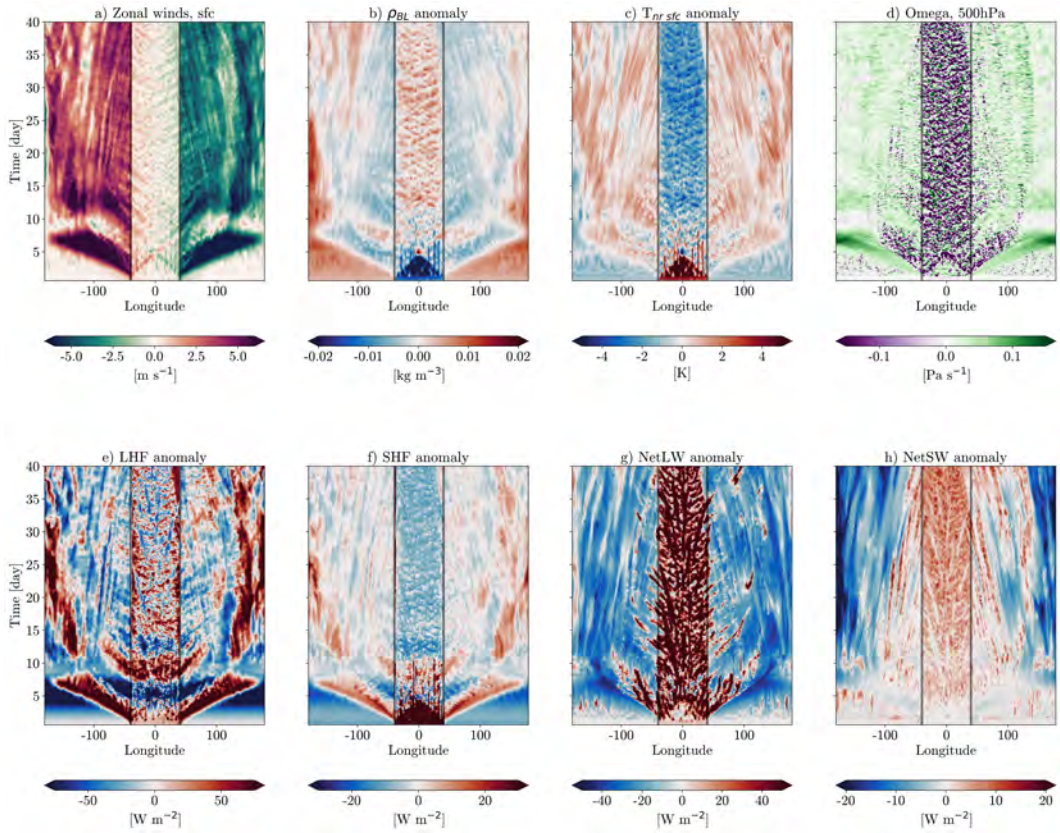

Figure 3: Hovmöller plots of a) Surface zonal winds, b) Density anomaly averaged over the boundary layer (lowest 1km) c) Near-surface temperature anomaly d) Omega at 500 hPa, e) Latent heat flux anomaly, f) Sensible heat flux anomaly, g) NetLW anomaly, h) NetSW anomaly, over the first 40 days of an RCE simulation with land, taken as a zonal slice through latitude=0°. The black lines show the coasts of the island. NetLW = LW_{sfc} - LW_{toa}, NetSW = SW_{toa} - SW_{sfc}, where LW_{sfc}/SW_{sfc} are the net longwave/shortwave fluxes at the surface and LW_{toa}/SW_{toa} are the net longwave/shortwave fluxes at the top of atmosphere. Positive fluxes are defined upwards. Anomalies are calculated from the horizontal mean.

These gradients drive the temperature gradient in Figure 4c and are responsible for driving the maintenance of the global circulation. This mechanism is the same as is discussed in previous studies (e.g. Wing et al., 2017). The shortwave heating anomalies show a pattern one would expect - negative anomalies in the lower troposphere representing the effects of cloud shielding and positive anomalies in the upper troposphere due to absorption by water vapour. However, the overall radiative heating anomaly pattern is driven by the longwave radiative feedbacks (Figure 4f). We hypothesise that these radiative heating anomalies are responsible for maintaining the island-centered circulation and therefore maintaining the aggregation of convection over the island.

3.2 Mechanism denial tests: Can land aggregation occur in the absence of radiative flux anomalies?

In order to test our radiative heating hypothesis, we perform some mechanism denial tests. These tests involve horizontally homogenizing the radiative heating rates at each model level, and each time step. This allows the radiative heating rates to change through time, but removes the horizontal gradients, thought to be responsible for maintaining the aggregation of convection (Muller & Held, 2012). Figure 5a shows that that homogenizing the shortwave fluxes has had little impact on the overall degree of aggregation, whereas homogenizing the longwave fluxes has decreased the degree of aggregation to the same as the NoLand-NotAggregated experiment. If we inspect the first 40 days of the simulations more closely (Figure 5b) then we can see that the CRH variance increases similarly in the first 7 days of each simulation with land, then it is after this that the degree of aggregation drops in the simulation with homogenized longwave feedbacks. This supports the findings in the previous section that the surface fluxes are driving the spin up of the circulation, with longwave feedbacks taking over as the dominant feedback after this.

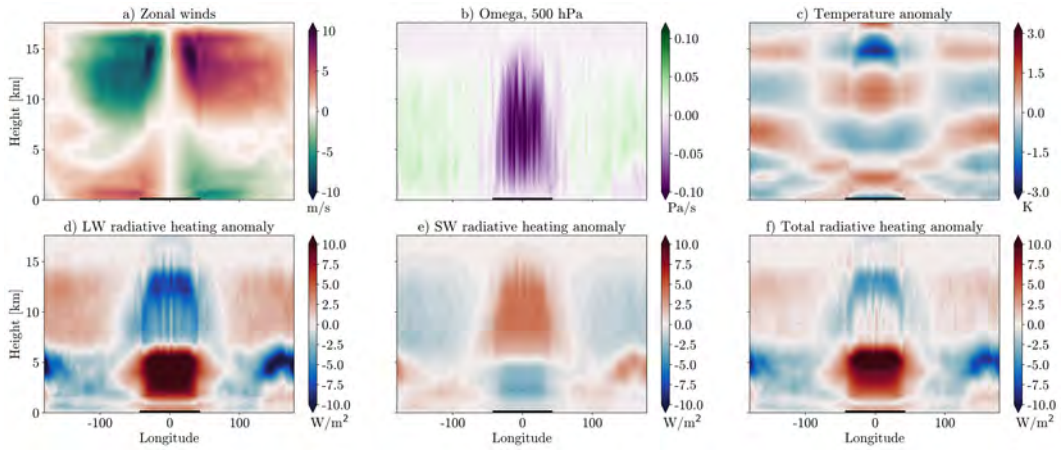

Figure 4: a) Zonal winds, b) Omega, c) Temperature anomaly, d) Longwave radiative heating anomaly, e) Shortwave radiative heating anomaly, and f) Total radiative heating anomaly zonal slices taken at latitude=0°, averaged over days 100-720 of the RCE simulation with land. Island is located between longitudes ±40°. Anomalies are calculated from the horizontal mean. Thick black line on the x-axis shows the horizontal island extent.

Figures 5c, d, and e present the same domain-mean properties as in Figure 2. Here, as in Figure 5a, the simulation with homogenized shortwave feedbacks mirrors the simulation with no homogenization, and the simulation with homogenized longwave feedbacks mostly mirrors the NoLand-NotAggregated simulation with no land. This also implies that the large domain-mean effects we see in Figure 2 are due to the aggregation process, not due to the inclusion of land itself.

The results from Figure 5b suggest that the circulation that is triggered in Figure 3 would also be triggered in the absence of longwave feedbacks, but that it is not being maintained, as we are no longer seeing any implied convective aggregation. Indeed, if we study how the same physical quantities act in the simulation without longwave feedbacks (Figure 6) we can see that this is true. The same circulation spin up can be seen by the land-sea thermal contrast in Figure 6c, and the subsequent gravity wave of subsidence in Figure 6d, however, without the convection triggering longwave feedbacks over the island, this circulation cannot be maintained, and instead the horizontal motion is now being dominated by wave-like motions across the globe (Figure 6a). This wave also travels at roughly 30 ms^{-1},

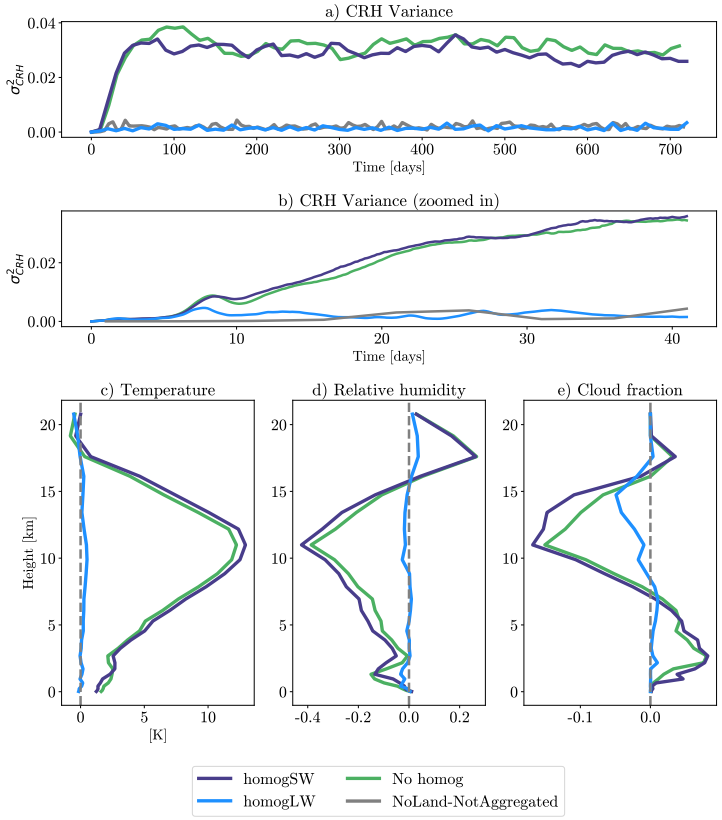

Figure 5: a), b) Time evolution of variance of domain-mean column relative humidity (CRH; σ^2_{CRH}). c)-e): Domain-mean vertical profiles of c) temperature, d) relative humidity, e) cloud fraction, time-averaged over days 100-720 of the simulations. In all plots, green lines represent a aggregated RCE simulation with land and fully interactive radiative fluxes ('no homog'), purple lines represent an RCE simulation with land where shortwave fluxes are horizontally homogenized at each time step ('homogSW'), blue lines represent an RCE simulation with land where longwave fluxes are horizontally homogenized at each time step ('homogLW'), and grey lines represent a non-aggregated simulation with no land ('NoLand-NotAggregated'). For figures c)-e), the vertical profiles from the non-aggregated simulation are subtracted from the 'No homog', 'homogLW', and 'homogSW' aggregated simulations' profiles.

as in our original simulation. These waves travel away from the island, passing through each other at the island's antipode, creating a circulation which alternates between land-centered and ocean-centered and repeats periodically approximately every 15-25 days. At the points of strongest surface-level divergence away from the island (for example, around day 20 in Figure 6a), the surface windspeeds over land increase, creating a warm, dry anomaly over the center of the island, above which there is clear-sky (Figure 6h). This point dries due to the increased windspeeds and the subsidence associated with the diverging circulation, and warms because of the increased surface shortwave absorption due to the clear-sky above as well as the increased windspeeds again. This warm anomaly then triggers new convection, resulting in the same thermally-driven circulation and subsequent gravity wave mechanism discussed. Over the island, convection tends to persist, except during the brief suppression period at the peak of the ocean-centered circulation. Whilst this still appears to provide a relatively visually aggregated scene in Figure 6h, the lack of persistent land-centered circulation means that the moisture field doesn't separate into extremely moist and extremely dry patches, as is synonymous with convective aggregation (Figure 5a; Bretherton et al. 2005; Muller & Held 2012), and that convection is not therefore fully suppressed away from the island, as in our original simulation (Figure 1). This wave-like motion across the atmosphere is nicely illustrated in the supplementary movie S2 of OLR and CRH. These results were also tested for simulations which were started from the equilibrium aggregated state shown in Figure 1, and then had the longwave heating rates homogenized. The results for this were the same as in Figure 5 and 6, and can be seen in Figure S2.

3.3 Sensitivity to island size

In order to test our results' sensitivity to the island size, we ran an ensemble of simulations where the island radius was increased from 10° to 80° in 10° increments. The winds, near-surface temperature, OLR and CRH Hovmöller plots for these experiments are shown in Figure 7. The standard result we've seen in this study, that convection will preferentially

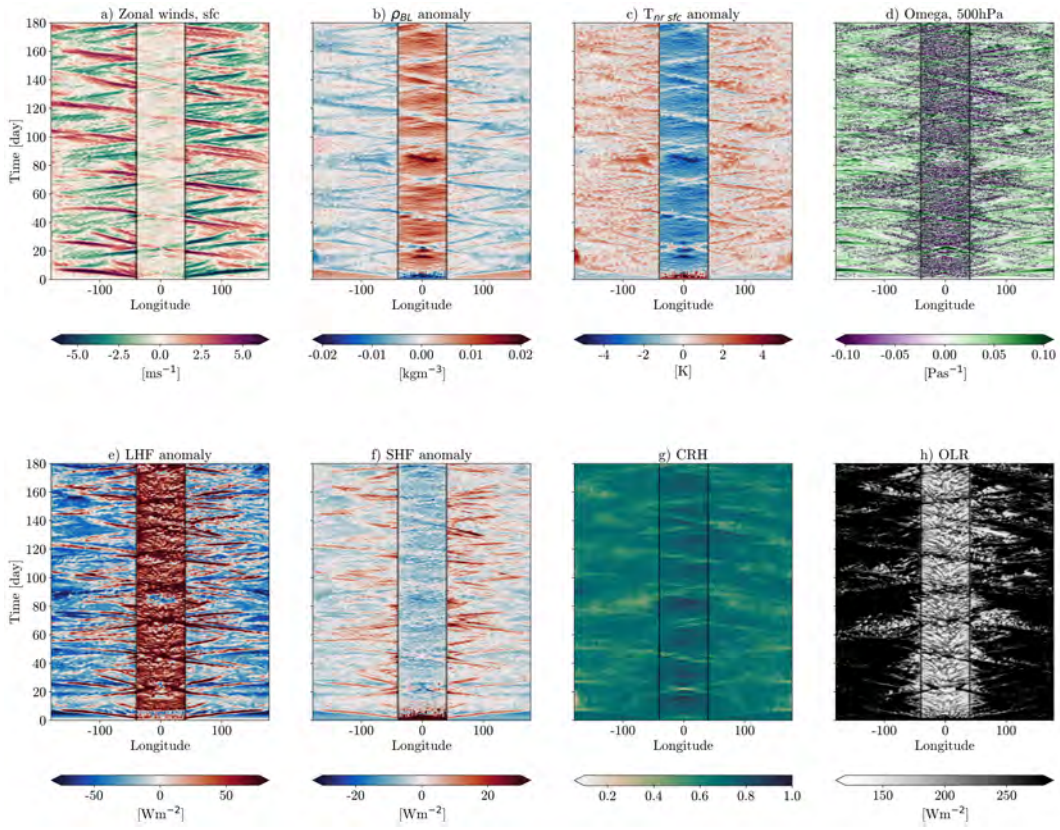

Figure 6: Hovmöller plots of a) Surface zonal winds, b) Density anomaly averaged over the boundary layer (lowest 1km) c) Near-surface temperature anomaly d) Omega at 500 hPa, e) Latent heat flux anomaly, f) Sensible heat flux anomaly, g) Column relative humidity, h) Outgoing longwave radiation, over the first 180 days of an RCE simulation with land where longwave fluxes are horizontally homogenized at each timestep, taken as a zonal slice through latitude=0°. The black lines show the coasts of the island. Anomalies are calculated from the horizontal mean.

form over the island, forced by a large thermally-driven circulation mostly holds at all island sizes. The extent of the circulation is much smaller in the 10° island simulation, as are the maximum horizontal windspeeds. This circulation extent grows, reaching across almost the whole globe in the simulations with island sizes between 20° and 50°. Along with this the convective cluster also grows to cover the whole island, leading to cool near-surface temperature anomalies over the island, due to the cloud shielding effect. Interestingly, above 50° the circulation stops growing in extent, and the convective cluster stops growing in size. At 60°, 70°, and 80° the convective cluster stays mostly the same size as the cluster in the 50° simulation, and so is no longer covering the whole island. This results in clear sky patches around the convective cluster, leading to large near-surface temperature anomalies. There is also a reduction in the horizontal extent of the zonal winds. We speculate that these results could point to a maximum size of aggregation cluster which would cover approximately 20% of the globe. Theories have previously been developed to try and explain the spatial scale of aggregation (Beucler & Cronin, 2019; D. Yang, 2018b; Arnold & Putman, 2018). These have typically pointed to the importance of boundary layer processes on controlling this spatial scale, and D. Yang (2018b) found that a typical length-scale of self-aggregation is $\mathcal{O}(2000km)$. The maximum length-scale of aggregation in our simulations is larger than this ($\mathcal{O}(10000km)$), however we speculate that this is likely due to the large forcing which the island is providing in these simulations. Interestingly, the typical scale of the MJO, a phenomenon that has previously been linked to convective aggregation (Arnold & Randall, 2015; Khairoutdinov & Emanuel, 2018), is also $\mathcal{O}(10000km)$. Nevertheless, these results could provide a new environment in which to further investigate the spatial scale of aggregation, especially looking towards how aggregation might manifest in the real world.

4 Discussion and Conclusions

Using the ICON GCM, we ran RCE experiments which included a large, continentally sized island to investigate how the inclusion of land affects the phenomenon of convective

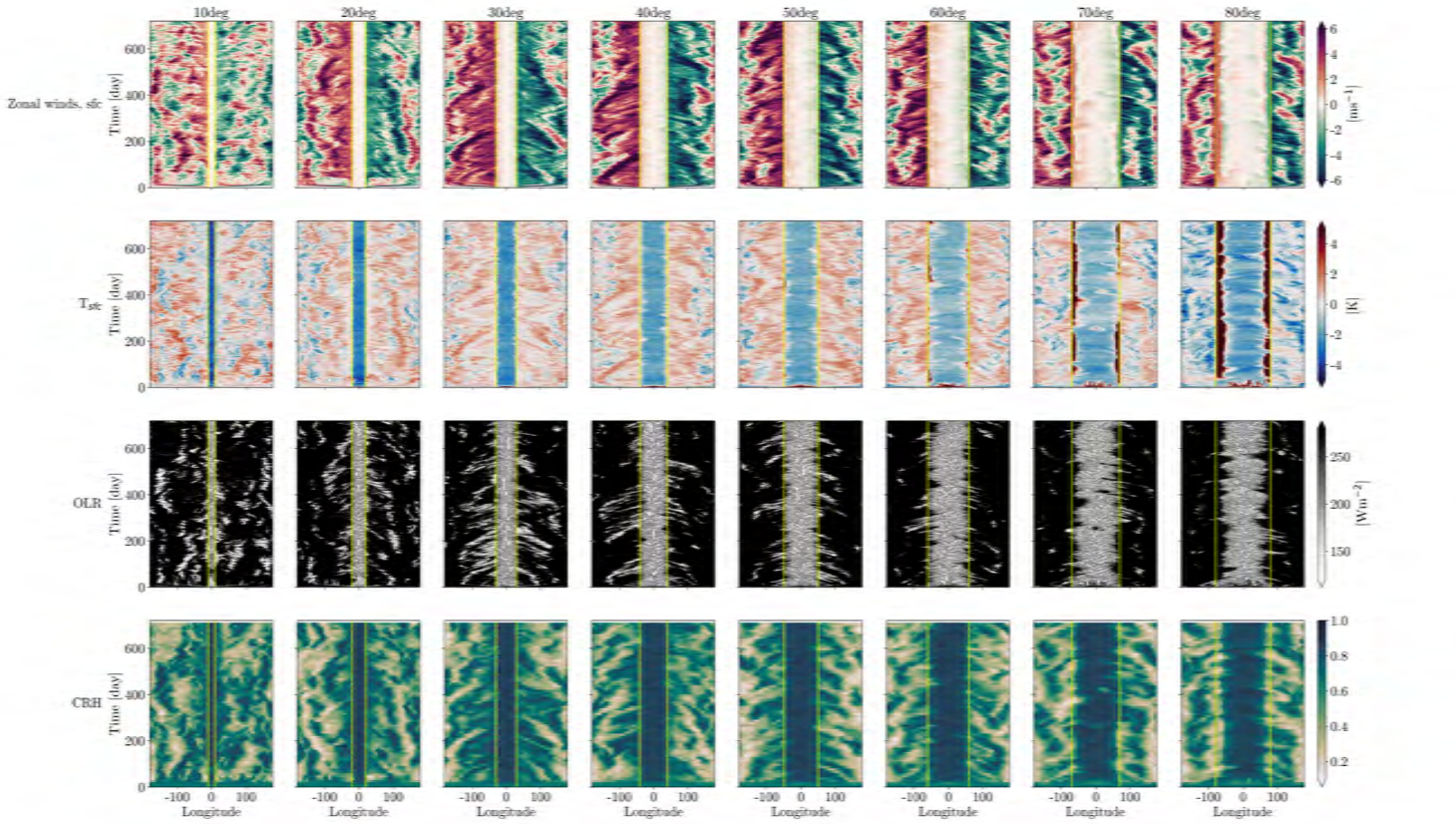

Figure 7: Hovmöller plots of a)-h) Surface zonal winds, i)-p) Near-surface temperature anomaly, q)-x) Outgoing longwave radiation, y)-Ff) Column relative humidity for 720 days RCE simulations with different land sizes. Land sizes increase from 10° (column 1) to 80° (column 8) in 10° increments. Anomalies are calculated from the horizontal mean.

aggregation. The island here represents a tropical rainforest-like land mass, with no elevation and no large-scale imposed winds, surrounded by a constant SST of 305K.

We showed that the inclusion of an idealized island in these global RCE simulations causes the convection to aggregate persistently over the island. This aggregation takes approximately 5-10 days to form spatially, however, it takes closer to 70 days for the model to reach statistical equilibrium, and therefore for the maximum degree of aggregation to be reached. The forced aggregation in these simulations causes similar domain-mean effects as self-aggregation has been shown to have before. This includes a domain-mean warming, free-tropospheric drying and a reduction in the high cloud amount comparatively to a non-aggregated simulation (e.g. Bretherton et al., 2005; Coppin & Bony, 2015; Wing & Cronin, 2016; Cronin & Wing, 2017). One key difference between self-aggregation, and this land-forced aggregation is the domain-mean temperature profile. As in Cronin et al. (2015), we find that aggregation over the island causes a large increase in the domain-mean temperature, much greater than the temperature increase seen in a self-aggregated simulation (Figure 2). This is due to a warmer cloud-base temperature in the land simulation, which drives the convection onto a warmer moist adiabat. This warmer moist adiabat is then propagated to the rest of the domain through convectively-triggered gravity waves.

The aggregation seen in these simulations is forced by a large-scale thermally-driven circulation. We showed that the circulation is initially triggered by a strong land-sea thermal contrast at the surface, causing surface wind convergence. This circulation mirrors the manifestation of a sea-breeze circulation, which has been shown to have important impacts on convection and precipitation over tropical islands, particularly in the Maritime Continent (Miller et al., 2003; Leutwyler & Hohenegger, 2021). In our simulations, we found that the sea-breeze circulation triggers convection, first at the edge of the island before being triggered increasingly inland. This convection then incites a gravity wave, moving at approximately 30 ms^{-1} outwards from the island. Gravity wave induced subsidence dries the columns

furthest away from the island, which forms large gradients in the CRH. Once these moisture gradients form, radiative feedbacks start to dominate the maintenance of the circulation with the strong longwave heating within the cloud layer combined with longwave cooling from the low emission temperature at the top of the cloud layer driving this maintenance. We have shown that this radiatively-driven circulation then persists throughout the simulation, despite negative near-surface temperature anomalies over the island.

We tested these results through mechanism denial experiments, which confirms the importance of longwave feedbacks for both the formation and maintenance of aggregation. When longwave heating rates are horizontally homogenized, aggregation no longer forms and the large-scale circulation is no longer be maintained. Instead, horizontal motion becomes dominated by gravity waves moving radially away from the island, causing a reversal of the land-sea circulation after the waves pass through each other at the island's antipode. This happens periodically throughout the simulation, with the waves converging on the island approximately every 15-25 days. With the lack of a constantly subsiding region away from the island, moisture gradients synonymous with aggregation do not form. Longwave feedbacks being essential for self-aggregation is a result that has been shown previously (e.g. Wing & Emanuel, 2014; Coppin & Bony, 2015; D. Yang, 2018a; Muller & Held, 2012). This study extends current understanding by demonstrating that even when land is included in an RCE model and could therefore change the mechanisms of aggregation through an increased importance of surface fluxes, longwave feedbacks are still the most important mechanism for driving and maintaining the aggregation of convection.

The results we have presented in this paper mostly scale with island size, until islands have a radius greater than 50° with the large-scale circulation roughly increasing in extent with island size, and the resulting convective cluster always covering the entire island. For experiments with an island radius greater than 50° the convective cluster never grows any greater than roughly 20% of coverage of the globe. This could point to a maximum size of

aggregation, something that has been a recent topic of interest (Beucler & Cronin, 2019; D. Yang, 2018b; Arnold & Putman, 2018). We highlight that the framework used in this study could provide some interesting insights to this work concerning the spatial-scale of aggregation.

We present this paper as an investigation of the impacts land-sea contrasts have on convective aggregation in a global configuration, and provide it as a useful addition to the growing literature on connecting idealized aggregation studies to the manifestation of real-world convective organization (e.g. Tompkins, 2001; Shamekh et al., 2020a; Müller & Hohenegger, 2020; Hohenegger & Stevens, 2016, 2018; Becker & Wing, 2020; Bony et al., 2020; Arnold & Randall, 2015; Muller & Romps, 2018; Beucler et al., 2020). We have shown that, whilst the shape and scale of aggregation change when a continentally-sized island is included in an idealised RCE world, many of the features of aggregation remain the same, including its effects on the large-scale environment and the feedbacks driving the formation and maintenance of aggregation. We have highlighted the key role that gravity waves play in shaping atmospheric circulations in RCE experiments in the absence of essential aggregation feedbacks. It can be difficult to draw conclusions on how results shown in this and other similar papers might be manifested in the real-world, due to the experiment's highly idealized configuration. To that end, there are many extensions to this paper that we feel will help to further elucidate the relationship between idealized aggregation and it's real-world manifestations, including investigating the effects of the diurnal cycle, SST gradients and rotation on the results presented here.

Acknowledgments

B. D. acknowledges funding from the Natural Environment Research Council, Oxford DTP, Award NE/L002612/1. G. D. is supported by the Israeli Science Foundation Grant (1419/21). G. D, P. S., and R. H. were also supported by the European Research Council (ERC) project constRaining the EffeCts of Aerosols on Precipitation (RECAP) under the Euro-

pean Union's Horizon 2020 research and innovation programme with grant agreement no. 724602. P. S. additionally acknowledges funding from the FORCeS and NextGEMs projects under the European Union's Horizon 2020 research program with grant agreements 821205 and 101003470, respectively. Computations and data processing have been performed on the ARCHER2 and JASMIN computing facilities. We also thank Cathy Hohenegger for the fruitful discussions during the preparation of this paper. We thank the Centre for Environmental Data Analysis (CEDA) Archive for hosting our model output data, which is freely available in NetCDF format online at (URL will be provided on paper acceptance).

References

Arnold, N. P., & Putman, W. M. (2018). Nonrotating convective self-aggregation in a limited area AGCM. *Journal of advances in modeling earth systems*, *10*(4), 1029–1046.

Arnold, N. P., & Randall, D. A. (2015). Global-scale convective aggregation: Implications for the Madden-Julian Oscillation. *Journal of Advances in Modeling Earth Systems*, *7*(4), 1499–1518. doi: 10.1002/2015MS000498

Becker, T., & Wing, A. A. (2020). Understanding the extreme spread in climate sensitivity within the radiative-convective equilibrium model intercomparison project. *Journal of Advances in Modeling Earth Systems*, *12*(10), e2020MS002165. doi: 10.1029/2020MS002165

Beucler, T., & Cronin, T. (2019). A budget for the size of convective self-aggregation. *Quarterly Journal of the Royal Meteorological Society*, *145*(720), 947–966.

Beucler, T., Leutwyler, D., & Windmiller, J. M. (2020). Quantifying convective aggregation using the tropical moist margin's length. *Journal of Advances in Modeling Earth Systems*, *12*(10), e2020MS002092. doi: 10.1029/2020MS002092

Bony, S., Semie, A., Kramer, R. J., Soden, B., Tompkins, A. M., & Emanuel, K. A. (2020). Observed modulation of the tropical radiation budget by deep convective organization and lower-tropospheric stability. *AGU advances*, *1*(3), e2019AV000155. doi: 10.1029/

2019AV000155

Bretherton, C. S., Blossey, P. N., & K., M. (2005). An energy-balance analysis of deep convective self-aggregation above uniform SST. *Journal of the Atmospheric Sciences*. doi: 10.1175/JAS3614.1

Coppin, D., & Bellon, G. (2019). Physical mechanisms controlling the offshore propagation of convection in the tropics: 1. flat island. *Journal of Advances in Modeling Earth Systems*, *11*(9), 3042–3056. doi: 10.1029/2019MS001793

Coppin, D., & Bony, S. (2015). Physical mechanisms controlling the initiation of convective self-aggregation in a General Circulation Model. *Journal of Advances in Modeling Earth Systems*, *7*(4), 2060–2078. doi: 10.1002/2015MS000571

Cronin, T. W., Emanuel, K. A., & Molnar, P. (2015). Island precipitation enhancement and the diurnal cycle in radiative-convective equilibrium. *Quarterly Journal of the Royal Meteorological Society*, *141*(689), 1017–1034. doi: 10.1002/qj.2443

Cronin, T. W., & Wing, A. A. (2017). Clouds, circulation, and climate sensitivity in a radiative-convective equilibrium channel model. *Journal of Advances in Modeling Earth Systems*, *9*(8), 2883–2905. doi: 10.1002/2017MS001111

Davis, C. A. (2015). The formation of moist vortices and tropical cyclones in idealized simulations. *Journal of the Atmospheric Sciences*, *72*(9), 3499–3516.

Dingley, B., Dagan, G., & Stier, P. (2021). Forcing convection to aggregate using diabatic heating perturbations. *Journal of Advances in Modeling Earth Systems*, *13*(10), e2021MS002579.

Giorgetta, M. A., Brokopf, R., Crueger, T., Esch, M., Fiedler, S., Helmert, J., ... Stevens, B. (2018). ICON-A, the atmosphere component of the ICON Earth System Model: I. model description. *Journal of Advances in Modeling Earth Systems*, *10*(7), 1613–1637. doi: 10.1029/2017MS001242

Hagemann, S. (2002). *An improved land surface parameter dataset for global and regional*

climate models (Tech. Rep.). Hamburg, Germany: Max Planck Institute for Meteorology.

Held, I. M., Hemler, R. S., & Ramaswamy, V. (1993). Radiative-convective equilibrium with explicit two-dimensional moist convection. *Journal of the Atmospheric Sciences*, *50*(23), 3909–3927. doi: 10.1175/1520-0469(1993)050⟨3909:RCEWET⟩2.0.CO;2

Hohenegger, C., & Stevens, B. (2016). Coupled radiative convective equilibrium simulations with explicit and parameterized convection. *Journal of Advances in Modeling Earth Systems*, *8*(3), 1468–1482.

Hohenegger, C., & Stevens, B. (2018). The role of the permanent wilting point in controlling the spatial distribution of precipitation. *Proceedings of the National Academy of Sciences*, *115*(22), 5692–5697. doi: 10.1073/pnas.1718842115

Holloway, C. E., & Woolnough, S. J. (2016). The sensitivity of convective aggregation to diabatic processes in idealized radiative-convective equilibrium simulations. *Journal of Advances in Modeling Earth Systems*, *8*(1), 166–195.

Jakob, C., Singh, M. S., & Jungandreas, L. (2019). Radiative convective equilibrium and organized convection: An observational perspective. *Journal of Geophysical Research: Atmospheres*, *124*(10), 5418–5430. doi: 10.1029/2018JD030092

Jungclaus, J. H., Lorenz, S. J., Schmidt, H., Brovkin, V., Brüggemann, N., Chegini, F., ... Claussen, M. (2022). The ICON Earth System Model version 1.0. *Journal of Advances in Modeling Earth Systems*, *14*(4), e2021MS002813. doi: https://doi.org/10.1029/2021MS002813

Khairoutdinov, M. F., & Emanuel, K. A. (2013). Rotating radiative-convective equilibrium simulated by a cloud-resolving model. *Journal of Advances in Modeling Earth Systems*, *5*(4), 816–825.

Khairoutdinov, M. F., & Emanuel, K. A. (2018). Intraseasonal variability in a cloud-permitting near-global equatorial aquaplanet model. *Journal of the Atmospheric Sciences*, *75*(12), 4337–4355.

589 Leutwyler, D., & Hohenegger, C. (2021). Weak cooling of the troposphere by tropical
590 islands in simulations of the radiative-convective equilibrium. *Quarterly Journal of the*
591 *Royal Meteorological Society*, *147*(736), 1788–1800.
592 Lohmann, U., & Roeckner, E. (1996). Design and performance of a new cloud microphysics
593 scheme developed for the ECHAM general circulation model. *Climate Dynamics*, *12*(8),
594 557–572. doi: 10.1007/BF00207939
595 Madden, R. A., & Julian, P. R. (1994). Observations of the 40–50-day tropical oscillation—a
596 review. *Monthly weather review*, *122*(5), 814–837. doi: 10.1175/1520-0493(1994)122⟨0814:
597 OOTDTO⟩2.0.CO;2
598 Manabe, S., & Wetherald, R. T. (1967). Thermal equilibrium of the atmosphere with a
599 given distribution of relative humidity. *Journal of Atmospheric Sciences*, *24*, 241–259.
600 doi: 10.1175/1520-0469(1967)024⟨0241:TEOTAW⟩2.0.CO;2
601 Miller, S. T. K., Keim, B. D., Talbot, R. W., & Mao, H. (2003). Sea breeze: Structure,
602 forecasting, and impacts. *Reviews of geophysics*, *41*(3). doi: 10.1029/2003RG000124
603 Muller, C. J., & Bony, S. (2015). What favors convective aggregation and why? *Geophysical*
604 *Research Letters*, *42*(13), 5626–5634. doi: 10.1002/2015GL064260
605 Muller, C. J., & Held, I. (2012). Detailed investigation of the self-aggregation of convection
606 in cloud-resolving simulations. *Journal of the Atmospheric Sciences*, *69*(8), 2551–2565.
607 doi: 10.1175/JAS-D-11-0257.1
608 Muller, C. J., & Romps, D. M. (2018). Acceleration of tropical cyclogenesis by self-
609 aggregation feedbacks. *Proceedings of the National Academy of Sciences*, *115*(12), 2930–
610 2935.
611 Müller, S. K., & Hohenegger, C. (2020). Self-aggregation of convection in spatially vary-
612 ing sea surface temperatures. *Journal of Advances in Modeling Earth Systems*, *12*(1),
613 e2019MS001698.
614 Naumann, A. K., Stevens, B., Hohenegger, C., & Mellado, J. P. (2017). A conceptual model

615 of a shallow circulation induced by prescribed low-level radiative cooling. *Journal of the*
616 *Atmospheric Sciences*, *74*(10), 3129–3144.
617 Nordeng, T.-E. (1994). *Extended versions of the convective parametrization scheme at*
618 *ECMWF and their impact on the mean and transient activity of the model in the tropics.*
619 doi: 10.21957/e34xwhysw
620 Popke, D., Stevens, B., & Voigt, A. (2013). Climate and climate change in a radiative-
621 convective equilibrium version of ECHAM6. *Journal of Advances in Modeling Earth*
622 *Systems*, 1–14. doi: 10.1029/2012MS000191@10.1002/(ISSN)1942-2466.MPIESM1
623 Popp, M., & Bony, S. (2019). Stronger zonal convective clustering associated with a wider
624 tropical rain belt. *Nature communications*, *10*(1), 1–12. doi: 10.1038/s41467-019-13645
625 -w
626 Reick, C. H., Gayler, V., Goll, D., Hagemann, S., Heidkamp, M., Nabel, J. E. M. S., ...
627 Wilkenskjeld, S. (2021). *JSBACH 3-the land component of the MPI earth system model:*
628 *documentation of version 3.2* (Tech. Rep.). Hamburg, Germany: Max Planck Institute
629 for Meteorology.
630 Reick, C. H., Raddatz, T., Brovkin, V., & Gayler, V. (2013). Representation of natural and
631 anthropogenic land cover change in MPI-ESM. *Journal of Advances in Modeling Earth*
632 *Systems*, *5*(3), 459–482.
633 Robe, F. R., & Emanuel, K. A. (2001). The effect of vertical wind shear on radiative–
634 convective equilibrium states. *Journal of the atmospheric sciences*, *58*(11), 1427–1445.
635 Roca, R., & Fiolleau, T. (2020). Extreme precipitation in the tropics is closely associated
636 with long-lived convective systems. *Communications Earth & Environment*, *1*(1), 1–6.
637 doi: 10.1038/s43247-020-00015-4
638 Sato, T., Miura, H., Satoh, M., Takayabu, Y. N., & Wang, Y. (2009). Diurnal cycle
639 of precipitation in the tropics simulated in a global cloud-resolving model. *Journal of*
640 *Climate*, *22*(18), 4809–4826. doi: 10.1175/2009JCLI2890.1

Shamekh, S., Muller, C. J., Duvel, J.-P., & d'Andrea, F. (2020a). How do ocean warm anomalies favor the aggregation of deep convective clouds? *Journal of the Atmospheric Sciences*, *77*(11), 3733–3745.

Shamekh, S., Muller, C. J., Duvel, J.-P., & d'Andrea, F. (2020b). Self-aggregation of convective clouds with interactive sea surface temperature. *Journal of Advances in Modeling Earth Systems*, *12*(11), e2020MS002164. doi: 10.1029/2020MS002164

Sobel, A. H., Nilsson, J., & Polvani, L. M. (2001). The weak temperature gradient approximation and balanced tropical moisture waves. *Journal of the Atmospheric Sciences*, *58*(23), 3650–3665. doi: 10.1175/1520-0469(2001)058⟨3650:TWTGAA⟩2.0.CO;2

Stephens, G. L., Van Den Heever, S., & Pakula, L. (2008). Radiative–convective feedbacks in idealized states of radiative–convective equilibrium. *Journal of the Atmospheric Sciences*, *65*(12), 3899–3916.

Stevens, B., Giorgetta, M., Esch, M., Mauritsen, T., Crueger, T., Rast, S., ... others (2013). Atmospheric component of the MPI-M Earth system model: ECHAM6. *Journal of Advances in Modeling Earth Systems*, *5*(2), 146–172.

Sundqvist, H., Berge, E., & Kristjánsson, J. E. (1989). Condensation and cloud parameterization studies with a mesoscale numerical weather prediction model. *Monthly Weather Review*, *117*(8), 1641–1657. doi: 10.1175/1520-0493(1989)117⟨1641:CACPSW⟩2.0.CO;2

Tiedtke, M. (1989). A comprehensive mass flux scheme for cumulus parameterization in large-scale models. *Monthly Weather Review*, *117*(8), 1779–1800. doi: 10.1175/1520-0493(1989)117⟨1779:ACMFSF⟩2.0.CO;2

Tobin, I., Bony, S., & Roca, R. (2012). Observational evidence for relationships between the degree of aggregation of deep convection, water vapor, surface fluxes, and radiation. *Journal of Climate*, *25*(20), 6885–6904. doi: 10.1175/JCLI-D-11-00258.1

Tompkins, A. M. (2001). On the relationship between tropical convection and sea surface temperature. *Journal of climate*, *14*(5), 633–637.

Tompkins, A. M., & Craig, G. C. (1998). Radiative–convective equilibrium in a three-dimensional cloud-ensemble model. *Quarterly Journal of the Royal Meteorological Society*, *124*(550), 2073–2097. doi: 10.1002/qj.49712455013

Tompkins, A. M., & Semie, A. G. (2017). Organization of tropical convection in low vertical wind shears: Role of updraft entrainment. *Journal of Advances in Modeling Earth Systems*, *9*(2), 1046–1068. doi: 10.1002/2016MS000802

Wang, S., & Sobel, A. H. (2017). Factors controlling rain on small tropical islands: Diurnal cycle, large-scale wind speed, and topography. *Journal of the Atmospheric Sciences*, *74*(11), 3515–3532. doi: 10.1175/JAS-D-16-0344.1

Wing, A. A., Camargo, S. J., & Sobel, A. H. (2016). Role of radiative–convective feedbacks in spontaneous tropical cyclogenesis in idealized numerical simulations. *Journal of the Atmospheric Sciences*, *73*(7), 2633–2642.

Wing, A. A., & Cronin, T. W. (2016). Self-aggregation of convection in long channel geometry. *Quarterly Journal of the Royal Meteorological Society*, *142*(694), 1–15. doi: 10.1002/qj.2628

Wing, A. A., & Emanuel, K. A. (2014). Physical mechanisms controlling self-aggregation of convection in idealized numerical modeling simulations. *Journal of Advances in Modeling Earth Systems*, *6*(1), 59–74. doi: 10.1002/2013MS000269

Wing, A. A., Emanuel, K. A., Holloway, C. E., & Muller, C. J. (2017). Convective self-aggregation in numerical simulations: A review. *Shallow clouds, water vapor, circulation, and climate sensitivity*, 1–25. doi: 10.1007/978-3-319-77273-8_1

Wing, A. A., Reed, K. A., Satoh, M., Stevens, B., Bony, S., & Ohno, T. (2018). Radiative–convective equilibrium model intercomparison project. *Geoscientific Model Development*, *11*(2), 793–813. doi: 10.5194/gmd-11-793-2018

Wing, A. A., Stauffer, C. L., Becker, T., Reed, K. A., Ahn, M.-S., Arnold, N. P., ... others (2020). Clouds and convective self-aggregation in a multi-model ensemble of radiative-convective equilibrium simulations. *Journal of Advances in Modeling Earth Systems*,

694 e2020MS002138.

695 Yang, D. (2018a). Boundary layer diabatic processes, the virtual effect, and convective
696 self-aggregation. *Journal of Advances in Modeling Earth Systems*, *10*(9), 2163–2176. doi:
697 10.1029/2017MS001261

698 Yang, D. (2018b). Boundary layer height and buoyancy determine the horizontal scale of
699 convective self-aggregation. *Journal of the Atmospheric Sciences*, *75*(2), 469–478.

700 Yang, G.-Y., & Slingo, J. (2001). The diurnal cycle in the tropics. *Monthly Weather Review*,
701 *129*(4), 784–801. doi: 10.1175/1520-0493(2001)129⟨0784:TDCITT⟩2.0.CO;2

702 Zängl, G., R., D., Rípodas, P., & Baldauf, M. (2015). The ICON (ICOsahedral
703 Non-hydrostatic) modelling framework of DWD and MPI-M: Description of the non-
704 hydrostatic dynamical core. *Quarterly Journal of the Royal Meteorological Society*,
705 *141*(687), 563–579. doi: 10.1002/qj.2378